

Universality of Dzyaloshinskii-Moriya interaction effect over domain-wall creep and flow regimes

Duck-Ho Kim,¹ Sang-Cheol Yoo,^{1,2} Dae-Yun Kim,¹ Byoung-Chul Min,² and Sug-Bong Choe^{1†}

¹Department of Physics and Institute of Applied Physics, Seoul National University, Seoul, 08826, Republic of Korea.

²Center for Spintronics, Korea Institute of Science and Technology, Seoul, 02792, Republic of Korea.

†Correspondence to: sugbong@snu.ac.kr

Chirality causes diverse phenomena in nature such as the formation of biological molecules¹, antimatters², non-collinear spin structures³, and magnetic skyrmions⁴. The chirality in magnetic materials is often caused by the noncollinear exchange interaction, called the Dzyaloshinskii-Moriya interaction (DMI)^{5,6}. The DMI produces topological spin alignments such as the magnetic skyrmions⁴ and chiral domain walls (DWs)⁷⁻¹². In the chiral DWs, the DMI generates an effective magnetic field H_{DMI} ¹³, resulting in a peculiar DW speed variation in the DW creep regime¹⁴⁻¹⁶. However, the role of H_{DMI} over the different DW-dynamics regimes remains elusive, particularly due to recent observation of distinct behaviors between the creep and flow regimes¹⁷. We hereby demonstrate experimentally that the role of H_{DMI} is invariant over the creep and flow regimes. In the experiments, the pure DMI effect is quantified by decomposing the symmetric and antisymmetric contributions of the DW motion. The results manifest

that the antisymmetric contribution vanishes gradually across the creep and flow regimes, revealing that the symmetric contribution from H_{DMI} is unchanged. Though the DW dynamics is governed by distinct mechanisms, the present observation demonstrates the uniqueness of the DMI effect on the DWs over the creep and flow regimes.

The DMI^{5,6} has recently shed new light on prominence due to recent findings on the dynamics of magnetic chiral DWs⁷⁻¹². Up to recent, Je *et al.*¹⁴ demonstrated that, in the DW creep regime, H_{DMI} modifies the DW energy density and causes variation of the DW speed under the influence of an in-plane magnetic field H_{in} . Such H_{in} -dependence of the DW speed is found to be symmetric for inversion with respect to H_{DMI} ; thus, one can quantify the sign and magnitude of H_{DMI} by symmetry measurement of the DW speed with respect to H_{in} ^{14,15}. However, recently Jué *et al.*¹⁸ proposed that energy dissipation—called chiral damping—generates additional variation of the DW speed, which is antisymmetric for inversion with respect to H_{DMI} . Because of such sizeable antisymmetric contribution, the symmetry-based H_{DMI} determination becomes controversial in the DW creep regime. To avoid this controversial issue, Vaňatka *et al.*¹⁷ demonstrated that in the flow regime, symmetry-based H_{DMI} determination becomes possible, as the flow regime exhibits symmetric DW speed variation, possibly due to the formation of soliton-like Bloch-type DWs above the Walker breakdown¹⁹.

By developing another experimental scheme, we decompose the symmetric and antisymmetric contributions in the creep regime. This scheme is based on the fact that the symmetric and antisymmetric contributions exhibit distinct dependences on an out-of-plane magnetic field. The experimental results clearly show that the antisymmetric contribution gradually vanishes across the creep and flow regimes, while the symmetric contribution

remains unchanged, confirming the uniqueness of H_{DMI} across the creep and flow regimes.

For this study, we chose with weak perpendicular magnetic anisotropy (PMA) films because of their high mobility of field-driven DW motion²⁰. The field-driven DW speed v was then measured over a wide range from 5×10^{-4} to 20 m/s across the creep and flow regimes. Figure 1a plots v as a function of out-of-plane magnetic field H_z with in-plane magnetic field $H_x = 0$ mT. The black arrow in the figure indicates the DW depinning field H_{dep} , above which the DW exhibits a dissipative viscous motion with $v \propto H_z - H_{\text{dep}}$, as guided by the red line of the best linear fit. Therefore, this DW motion belongs to the flow regime ($H_z > H_{\text{dep}}$). On the other hand, the creep regime ($H_z < H_{\text{dep}}$) exhibits thermally activated DW motion with the creep criticality $\ln(v) \propto H_z^{-1/4}$, as guided by the blue line of the best linear fit in Fig. 1b.

The effect of H_x on the DW motion was then examined. Figures 2a-d show v/v_{min} with respect to H_x under various strengths of H_z , i.e., 1.9, 3.4, 17, and 41 mT, respectively, over the creep and flow regimes. Here, v_{min} is the apparent minimum of v as defined below. The best parabolic fitting (solid curve) is shown in each plot to guide the symmetry of v , indicating the in-plane magnetic field H_{min} (purple arrows) for v_{min} (i.e., $v_{\text{min}} \equiv v(H_{\text{min}})$). It is interesting to note that H_{min} is shifted across the plots with respect to the strength of H_z . Therefore, H_{min} of the creep regime (green dotted line) differs from that of the flow regime (blue dotted line). As the H_{DMI} -determination scheme is based on the measurement of the inversion symmetry with respect to H_{min} , this observation indicates that H_{DMI} cannot be uniquely determined irrespective of H_z . Because of better symmetries of $v(H_x)$ observed in the flow regime, Vaňatka *et al.*¹⁷ have argued that H_{min} measured in the flow regime truly quantifies H_{DMI} ($= -H_{\text{min}}$), whereas the asymmetric behavior in the creep

regime contains sizeable antisymmetric contribution.

To confirm whether H_{\min} measured in the flow regime corresponds to the true H_{DMI} , we further analyze the DW motion in the creep regime by decomposing the symmetric and antisymmetric contributions. The principle of the decomposition is as follows: recent studies^{14,21,22} have proposed that in the creep regime, the thermally activated DW motion follows the DW creep criticality²³ as given by $v(H_x, H_z) = v_0(H_x) \exp[-\alpha(H_x)H_z^{-1/4}]$, where v_0 is the characteristic speed and α is a scaling parameter related to the energy. According to ref.14, $\alpha(H_x)$ mainly attributes the symmetric contribution by varying the DW energy density. On the other hand, it has been proposed in ref.18 that $v_0(H_x)$ possibly includes a sizeable antisymmetric contribution, even though the nature of $v_0(H_x)$ is not fully understood yet. The troublesome $v_0(H_x)$ can be easily removed experimentally by measuring two $v(H_x)$ s under the influence of different out-of-magnetic field biases, H_{z1} and H_{z2} ²⁴. The ratio R_{12} of these two $v(H_x)$ s is then written as

$$\ln[R_{12}(H_x)] = -\alpha(H_x)(H_{z1}^{-1/4} - H_{z2}^{-1/4}), \quad (1)$$

which contains only the symmetric contribution from $\alpha(H_x)$. Figure 2e plots $R_{12}(H_x)$ with $H_{z1} = 2.1$ mT and $H_{z2} = 1.9$ mT. The black curve in the plot is the best fit to guide the symmetry of R_{12} . The equations and parameters for the best fit will be discussed later. The figure clearly shows that the inversion symmetry axis of $R_{12}(H_x)$ becomes identical to that (blue dotted line) of the flow regime. This observation therefore supports the claims that the inversion symmetry axis of the flow regime corresponds to the true H_{DMI} and the present analysis method is valid to extract the symmetric contribution in the creep regime. Therefore, one can conclude that H_{DMI} can be uniquely determined for both creep and flow regimes. Hereafter, we will denote the uniquely determined H_{DMI} as H_{DMI}^* .

Similarly, $v_0(H_x)$ can be determined by using the relation

$$v_0(H_x) = v_1(H_x)/[R_{12}(H_x)]^\gamma, \quad (2)$$

where $\gamma \equiv H_{z1}^{-1/4}/(H_{z1}^{-1/4} - H_{z2}^{-1/4})$ and v_1 is the DW speed measured under H_{z1} . Figure 2f shows $v_0(H_x)$ determined with $H_{z1} = 2.1$ mT and $H_{z2} = 1.9$ mT. Though the data are slightly scattered since the statistical error in R_{12} is amplified greatly because of a large γ , the plot exhibits a noticeable variation in $v_0(H_x)$, as indicated by the solid line of the best linear fit. Such sizeable variation in $v_0(H_x)$ verifies that the antisymmetric contribution of the DW speed is mainly attributed to $v_0(H_x)$, since $\alpha(H_x)$ is solely responsible for the symmetric contribution. Such antisymmetric variation of $v_0(H_x)$ can be caused by several reasons such as chiral damping¹⁸, asymmetric DW width²⁵, or H_x -induced magnetization tilting inside the domains adjacent to the DWs. Presently, we are unable to distinguish these possibilities and further deliberate measurements are desired for future studies.

By use of H_{DMI}^* , the antisymmetric contributions can be further analyzed. Figure 3(a) plots the asymmetry A of the DW speed with respect to ΔH_x (i.e. $\Delta H_x \equiv H_x + H_{\text{DMI}}^*$) for the creep (red) and flow (blue) regimes, where

$$A(\Delta H_x) \equiv \frac{v(-H_{\text{DMI}}^* + \Delta H_x) - v(-H_{\text{DMI}}^* - \Delta H_x)}{v(-H_{\text{DMI}}^* + \Delta H_x) + v(-H_{\text{DMI}}^* - \Delta H_x)}. \quad (3)$$

It is clear from the figure that the creep regime exhibits a large asymmetry, in contrast with zero asymmetry in the flow regime. In the creep regime, one can readily derive the relation $A(\Delta H_x) \cong \beta \Delta H_x$ within the context of the creep criticality, where

$$\beta \equiv \frac{dv_0/d\Delta H_x|_{\Delta H_x=0}}{v_0(-H_{\text{DMI}}^*)}. \quad (4)$$

The value of β ($= 4.6 \pm 0.1 \text{ T}^{-1}$) determined from the red symbols of Fig. 3a exactly coincide with the value ($= 4.2 \pm 1.4 \text{ T}^{-1}$) determined from Fig. 2f within the experimental accuracy. The exact conformity again supports the validity of our approach.

Figure 3b summarizes the experimentally determined β (black) and H_{\min} (green) with respect to H_z . It is evident from the figure that there exist sizeable asymmetries in the creep regime with a small H_z , but the asymmetry quickly decays as H_z increases in the flow regime. Similarly, H_{\min} approaches $-H_{\text{DMI}}^*$ as H_z increases. The dotted lines indicate a simple exponential decay function.

According to ref.14, $\alpha(H_x) = \alpha_0[\sigma_{\text{DW}}(H_x)/\sigma_0]^{1/4}$, where σ_{DW} is the DW energy density, σ_0 is the Bloch-type DW energy density, and α_0 is a scaling constant. Recent studies^{14,15} on the DMI effect on DWs have revealed that $\sigma_{\text{DW}}(H_x)$ is given by

$$\sigma_{\text{DW}}(H_x) = \begin{cases} \sigma_0 - 2\lambda K_D \left| \frac{H_x + H_{\text{DMI}}^*}{H_K} \right|^2 & \text{for } |H_x + H_{\text{DMI}}^*| \leq H_K \\ \sigma_0 + 2\lambda K_D - 4\lambda K_D \left| \frac{H_x + H_{\text{DMI}}^*}{H_K} \right| & \text{otherwise} \end{cases}. \quad (5)$$

Here, K_D is the DW anisotropy energy density, λ is the DW width, and H_K ($\equiv 4K_D/\pi M_S$) is the DW anisotropy field. The solid line in Fig. 2e is the best fit by these equations with the following best fitting parameters: $\alpha_0 = 3.81 \text{ T}^{1/4}$, $\lambda K_D/\sigma_0 = 0.027$, $H_K = 29.7 \text{ mT}$, and $H_{\text{DMI}}^* = 59.3 \text{ mT}$. For the case in which v_0 exhibits a finite asymmetry i.e. $v_0(-H_{\text{DMI}}^* + \Delta H_x) \cong v_0(-H_{\text{DMI}}^*) + \beta \Delta H_x$, one can again easily calculate that the apparent minimum H_{\min} can be written as

$$H_{\min} \cong -H_{\text{DMI}}^* - \eta \beta H_z^{1/4}, \quad (6)$$

where $\eta \equiv \sigma_0 H_K^2 / \alpha_0 \lambda K_D$. The prediction given by Eq. (6) is experimentally confirmed as

observed by the linear relation between $\beta H_z^{1/4}$ and H_{\min} in Fig. 3c. Therefore, one can conclude that the asymmetry is the origin of the deviation in H_{\min} and therefore, H_{\min} converges to $-H_{\text{DMI}}^*$ as the asymmetry vanishes in the flow regime.

The DW motion in the flow regime can be described by the 1-dimensional DW model^{26,27} based on the Landau-Lifshitz-Gilbert (LLG) equation²⁸. It is well known that, under a H_z larger than the Walker breakdown field²⁹, the DW exhibits precessional motion³⁰. By solving the 1-dimensional DW model, the DW speed is given by $v = \lambda(\gamma_0 H_z - 2\pi/T)/\alpha_G$, where α_G is the Gilbert damping constant and γ_0 is the gyromagnetic ratio. The precession period T is then written as

$$T = \frac{1 + \alpha_G^2}{\gamma_0} \int_0^{2\pi} \frac{d\psi}{H_z - \alpha_G \frac{\pi}{2} (H_x + H_{\text{DMI}}) \sin \psi + \alpha_G \frac{\pi}{2} H_K \sin \psi \cos \psi}, \quad (7)$$

where ψ is the angle of the magnetization inside the DW. Since $H_z \gg \alpha_G H_K$ for the experimental condition in the flow regime with a small α_G , it is a good approximation to write T as

$$T \approx \frac{1 + \alpha_G^2}{\gamma_0} \int_0^{2\pi} \frac{d\psi}{H_z - \alpha_G \frac{\pi}{2} (H_x + H_{\text{DMI}}) \sin \psi} = \frac{1 + \alpha_G^2}{\gamma_0} \frac{2\pi}{\sqrt{H_z^2 - \alpha_G^2 \left(\frac{\pi}{2}\right)^2 (H_x + H_{\text{DMI}})^2}}. \quad (8)$$

Figure 4 plots the numerical evaluation T/T_{\min} of Eqs. (7) and (8) for our experimental condition, where T_{\min} is defined as T at $H_x = -H_{\text{DMI}}$. The micromagnetic simulation results by use of the object oriented micromagnetic framework (OOMMF) are plotted together. The figure clearly shows that all results match each other with accuracy better than

1%. Therefore, it is good to write v as

$$\begin{aligned}
v &\approx \frac{\lambda\gamma_0}{\alpha_G} \left(H_z - \frac{1}{1 + \alpha_G^2} \sqrt{H_z^2 - \alpha_G^2 \left(\frac{\pi}{2}\right)^2 (H_x + H_{\text{DMI}})^2} \right) \\
&\approx \frac{\lambda\gamma_0\alpha_G}{1 + \alpha_G^2} H_z \left(1 + \left(\frac{\pi}{2}\right)^2 \frac{(H_x + H_{\text{DMI}})^2}{2H_z^2} \right), \tag{9}
\end{aligned}$$

which exhibits symmetric behavior with a parabolic dependence on $H_x + H_{\text{DMI}}$. Note that the parabolic variation originates from the suppression of precessional DW motion because of the additional energy barrier enhanced by an in-plane magnetic field¹³. It is also worthwhile to note that λ also varies with respect to H_x ²⁵, but the variation of λ is expected to be less than a few tens of percent. Therefore, the large variation of v observed in Fig. 2d is mostly attributed to the suppression of the precessional DW motion rather than λ variation.

Finally, we would like to mention the possible antisymmetric contributions in the flow regime. Yoshimura *et al.*¹⁹ recently demonstrated that above the Walker breakdown, the DMI generates soliton-like DWs partitioned by vertical Bloch lines. These DWs stay in the Bloch type configuration without precession; therefore, all the effects related to the DW chirality such as the chiral damping¹⁸ and chiral λ variation²⁵ are expected to disappear. In addition, Kim *et al.*²⁵ have shown that the Bloch-type DWs have the same DW width and DW energy density irrespective of the strength of H_x . The H_x -induced magnetization tilting possibly causes additional variation in λ . However, because of the large anisotropy field (~ 1 T) in typical PMA films, the variation of λ is estimated to be small ($< 3\%$) within the range of H_x . Such a small variation of λ can cause small asymmetry ($< 5\%$), which causes a deviation of approximately 1.8 mT in H_{min} that is negligibly small in comparison with other experimental inaccuracies.

In conclusion, we examine the nature of the asymmetric behavior in DW motion over the creep and flow regimes. Based on the distinct dependence of the DW speed on the in-plane and out-of-plane magnetic fields, the symmetric and antisymmetric contributions of the DW speed are decomposed, enabling one to quantify the pure effect of the DMI. The results show that the antisymmetric contribution vanishes gradually across the regimes, while the symmetric contribution remains unchanged, confirming the uniqueness of the DMI-induced magnetic field across the regimes. The present observation elucidates the underlying physics on the recent puzzling issue in the DMI-related chiral DW dynamics.

References

1. Siegel, J. S. Single-handed cooperation. *Nature* **409**, 777-778 (2001).
2. Ellis, J. Antimatter matters. *Nature* **424**, 631-634 (2003).
3. Bode, M. *et al.* Chiral magnetic order at surfaces driven by inversion asymmetry. *Nature* **447**, 190-193 (2006).
4. Yu, X. Z., Onose, Kanazawa, Y. N., Park, J. H., Han, J. H., Matsui, Y., Nagaosa, N. & Tokura, Y. Real-space observation of a two-dimensional skyrmion crystal. *Nature* **465**, 901-904 (2010).
5. Dzialoshinskii, I. E. Thermodynamic theory of weak ferromagnetism in antiferromagnetic substances. *Sov. Phys. JETP* **5**, 1259-1272 (1957).
6. Moriya, T. Anisotropic superexchange interaction and weak ferromagnetism. *Phys. Rev.* **120**, 91-98 (1960).
7. Chen, G. *et al.* Novel chiral magnetic domain wall structure in Fe/Ni/Cu(001) films. *Phys. Rev. Lett.* **110**, 177204 (2013).
8. Ryu, K.-S., Thomas, L., Yang, S.-H. & Parkin, S. Chiral spin torque at magnetic domain walls. *Nature Nanotech.* **8**, 527-533 (2013).
9. Haazen, P. P. J., Murè, E., Franken, J. H., Lavrijsen, R., Swagten, H. J. M. & Koopmans, B. Domain wall depinning governed by the spin Hall effect. *Nature Mater.* **12**, 299-303 (2013).
10. Emori, S., Bauer, U., Ahn, S.-M., Martinez, E. & Beach, G. S. D. Current-driven dynamics of chiral ferromagnetic domain walls. *Nature Mater.* **12**, 611-616 (2013).

11. Yang, S.-H., Ryu, K.-S. & Parkin, S. Domain-wall velocities of up to 750 m s⁻¹ driven by exchange-coupling torque in synthetic antiferromagnets. *Nature Nanotech.* **10**, 221-226 (2015).
12. Moon, K.-W. *et al.* Magnetic bubblecade memory based on chiral domain walls. *Sci. Rep.* **5**, 9166 (2015).
13. Thiaville, A., Rohart, S., Jué, É., Cros, V. & Fert, A. Dynamics of Dzyaloshinskii domain walls in ultrathin magnetic films. *Europhys. Lett.* **100**, 57002 (2012).
14. Je, S.-G. *et al.* Asymmetric magnetic domain-wall motion by the Dzyaloshinskii-Moriya interaction. *Phys. Rev. B* **88**, 214401 (2013).
15. Hrabec, A. *et al.* Measuring and tailoring the Dzyaloshinskii-Moriya interaction in perpendicularly magnetized thin films. *Phys. Rev. B* **90**, 020402(R) (2014).
16. Pizzini, S. *et al.* Chirality-induced asymmetric magnetic nucleation in Pt/Co/AlOx ultrathin microstructures. *Phys. Rev. Lett.* **113**, 047203 (2014).
17. Vaňatka, M. *et al.* Velocity asymmetry of Dzyaloshinskii domain walls in the creep and flow regimes. *J. Phys.: Condens. Matter* **27**, 326002 (2015).
18. Jué, E. *et al.* Chiral damping of magnetic domain walls. *Nature Mater.* **15**, 272-277 (2016).
19. Yoshimura, Y. *et al.* Soliton-like magnetic domain wall motion induced by the interfacial Dzyaloshinskii–Moriya interaction. *Nature Phys.* **12**, 157-162 (2016).
20. Kim, D.-H. *et al.* Maximizing domain-wall speed via magnetic anisotropy adjustment in Pt/Co/Pt films. *Appl. Phys. Lett.* **104**, 142410 (2014).

21. Kim, K.-J. *et al.* Interdimensional universality of dynamic interfaces. *Nature* **458**, 740-742 (2009).
22. Metaxas, P. J. *et al.* Creep and flow regimes of magnetic domain-wall motion in ultrathin Pt/Co/Pt films with perpendicular anisotropy. *Phys. Rev. Lett.* **99**, 217208 (2007).
23. Lemerle, S. *et al.* Domain wall creep in an Ising ultrathin magnetic film. *Phys. Rev. Lett.* **80**, 849-852 (1998).
24. Kim, D.-Y., Kim, D.-H., Moon, J. & Choe, S.-B. Determination of magnetic domain-wall types using Dzyaloshinskii–Moriya-interaction-induced domain patterns. *Appl. Phys. Lett.* **106**, 262403 (2015).
25. Kim, D.-Y., Kim, D.-H. & Choe, S.-B. Intrinsic asymmetry in chiral domain walls due to the Dzyaloshinskii–Moriya interaction. *Appl. Phys. Express* **9**, 053001 (2016).
26. Slonczewski, J. C. *AIP Conf. Proc.* **5**, 170-174 (1972).
27. Hillebrands, B. & Thiaville, A. Spin Dynamics in Confined Magnetic Structures III, *Topics in Applied Physics* **101**, 161-205 (2006).
28. Gilbert, T. L. A phenomenological theory of damping in ferromagnetic materials. *IEEE Trans. Magn.* **40**, 3443-3449 (2004).
29. Beach, G. S. D., Nistor, C., Knutson, C., Tsoi, M. & Erskine, J. L. Dynamics of field-driven domain-wall propagation in ferromagnetic nanowires. *Nature Mater.* **4**, 741-744 (2005).

30. Hayashi, M., Thomas, L., Rettner, C., Moriya, R. & Parkin, S. S. P. Direct observation of the coherent precession of magnetic domain walls propagating along permalloy nanowires. *Nature Phys.* **3**, 21-25 (2007).

Figure Captions

Figure 1. **Plot of v as a function of H_z with $H_x = 0$.** **a**, Linear scale plot for the flow regime and **b**, creep scale plot for the creep regime. Both the blue and red lines show the best linear fit.

Figure 2. **Plot of v/v_{\min} with respect to H_x under various strengths of H_z :** **a**, 1.9 **b**, 3.4 **c**, 17, and **d**, 41 mT. In each plot, the solid line shows the best parabolic fit with Eq. (9) and the purple arrow indicates H_{\min} for v_{\min} . **e**, Plot of R_{12} with respect to H_x with $H_{z1} = 2.1$ mT and $H_{z2} = 1.9$ mT. The solid line shows the best fit with Eq. (5). **f**, Plot of v_0 with respect to H_x . The solid line shows the best linear fit.

Figure 3. **Asymmetry of the DW speed over the creep and flow regimes.** **a**, Plot of A with respect to ΔH_x for the creep (red) and flow (blue) regimes. The solid lines show the best linear fit. **b**, Plot of β (black) and H_{\min} (green) with respect to H_z . The dotted lines indicate a simple exponential decay function. **c**, Plot of $\beta H_z^{1/4}$ with respect to H_{\min} . The black solid line shows the best linear fit.

Figure 4 **Plot of T/T_{\min} with respect to H_x ,** calculated by Eq. (7) (solid line) and Eq. (8) (circular symbols) as well as by micromagnetic simulation (square symbols) at $H_z = 51$ mT.

Methods

Methods and any associated references are available in the online version of the paper.

Acknowledgements

This work was supported by a National Research Foundations of Korea (NRF) grant that was funded by the Ministry of Science, ICT and Future Planning of Korea (MSIP) (2015R1A2A1A05001698 and 2015M3D1A1070465). D.-H.K. was supported by a grant funded by the Korean Magnetics Society. B.-C.M. was supported by the KIST institutional program and Pioneer Research Center Program of MSIP/NRF (2011-0027905).

Author contributions

D.-H.K. planned and designed the experiment and S.-B.C. supervised the study. D.-H.K. and D.-Y.K. carried out the measurement. S.-C.Y. and B.-C.M. prepared the samples. S.-B.C. and D.-H.K. performed the analysis and wrote the manuscript. All authors discussed the results and commented on the manuscript.

Additional information

Correspondence and request for materials should be addressed to S.-B.C.

Competing financial interests

The authors declare no competing financial interests.

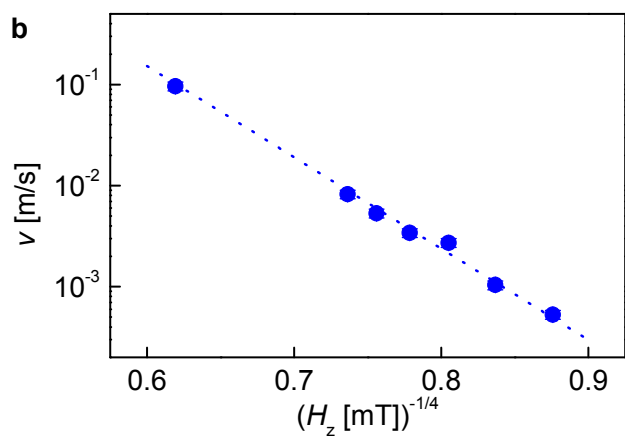
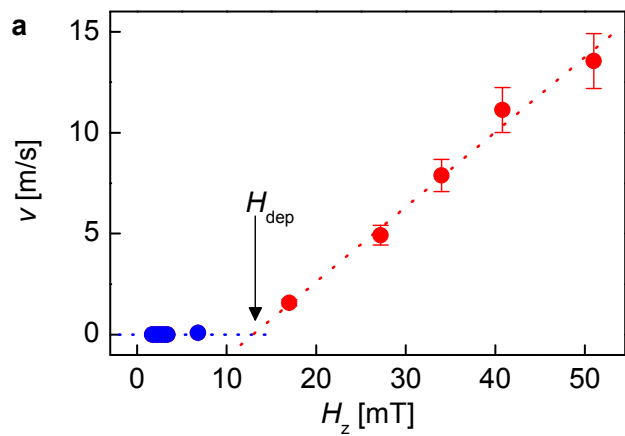


Figure 1

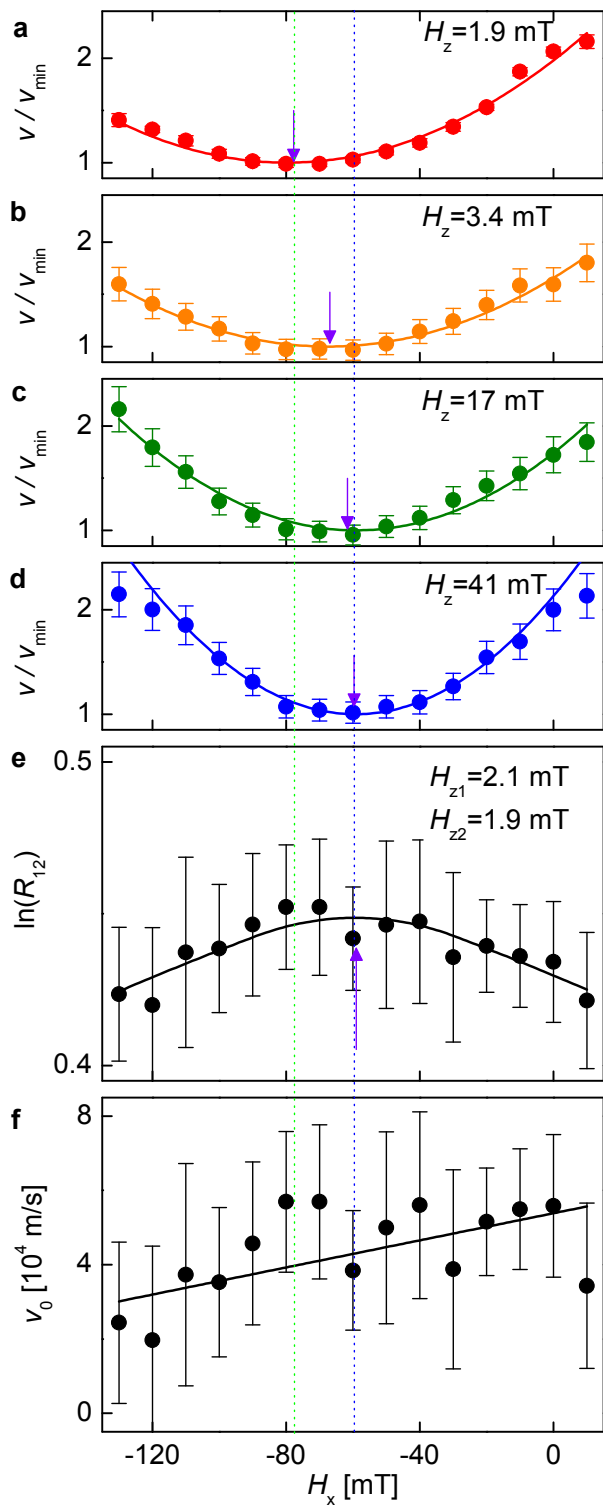


Figure 2

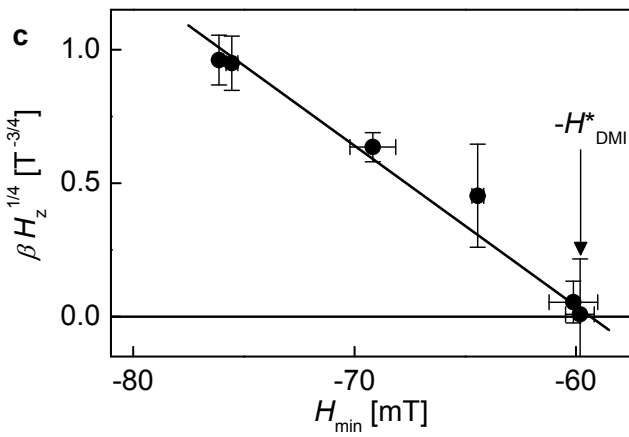
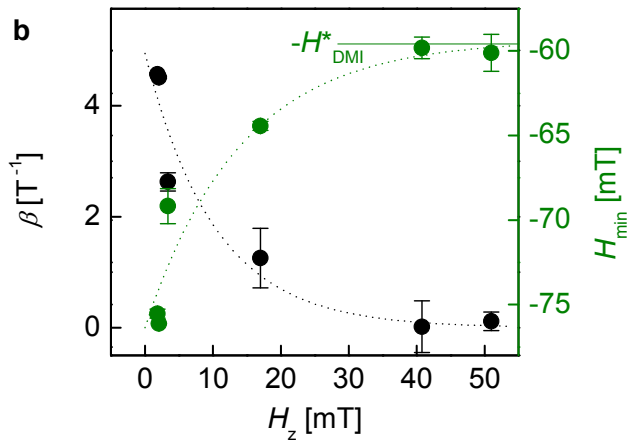
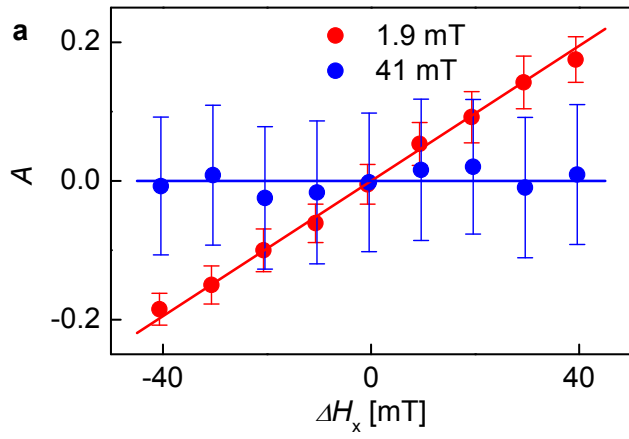


Figure 3

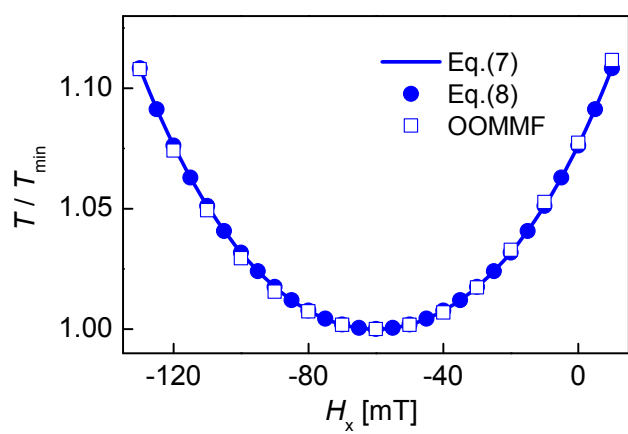


Figure 4